Enhanced suppression of draw resonance in sheet casting due to heating

Kam Chuen Ng[a] and Steven J. Weinstein[b]

Department of Chemical Engineering, Rochester Institute of Technology, 160 Lomb Memorial Drive, Rochester, NY 14623

(Dated: 17 March 2025)

We consider the effect of heating on the stability of a highly viscous and thin Newtonian sheet of liquid drawn onto a moving substrate under conditions of negligible inertia and gravity. Whereas the stability of the drawing process has been well-studied under conditions where the liquid sheet is isothermal or cooled, the effect of heating has not. We impose a Gaussian temperature profile in the liquid to mimic a process in which film moves through a heating zone over a portion of the sheet; this is followed by a region of cooling. Here, we show a remarkable suppression of the draw resonance instability by heating the sheet as it flows. Compared with an isothermal configuration, the critical draw ratio — defined as the maximum ratio of the final to initial velocity in the sheet below which the sheet is stable — can be increased by many orders of magnitude depending on parameters of the imposed Gaussian heating profile. A cooling profile that follows the Gaussian has a quantitative but relatively small effect on the magnitude of the critical draw ratio. We find that a relatively narrow region of heating relative to the sheet length can dramatically increase the critical draw ratio. Although results of this paper are provided predominantly in the limit of negligible heat transfer resistances, the effect of heat transfer on presented results is examined.

Keywords: Draw resonance, draw ratio, Newtonian liquid sheet, instability, liquid curtain, heating and cooling, Chebyshev collocation

[a]corresponding author; Electronic mail: kamchuenng@yahoo.com
[b]Electronic mail: sjweme@rit.edu

I. INTRODUCTION

Two-dimensional planar liquid sheets are commonly employed as an enabling step in the coating of liquid films on moving substrates. When used in high speed coating processes, these gradually thinning liquid sheets (often referred to as curtains) are inertia-dominated and essentially inviscid[30]; inertial curtain flows are used to suppress air entrainment through high stagnation pressures at the impingement location on the substrate[3]. The dynamics and stability of such flows have been well-studied[30] and remains a research area of active interest[1,6–8,15,28]. By contrast, extrusion coating[31] and film-casting/drawing processes[33] involve planar liquid sheets that are gradually thinning yet viscous dominated. The stability of these viscous sheets is well-known[5,11,22]; for a constant viscosity Newtonian sheet, an instability arises when the critical draw ratio — defined as the ratio of the liquid speed at the bottom of the curtain to its top — exceeds 20.21. This so-called "draw resonance instability" can occur in industrial applications involving molten materials, and thus the impact of cooling[13,23,25] has been previously studied. Prior work has included heat transfer resistances both within and outside of the fluid. The incorporation of inertia, gravity and surface tension on viscous-dominated non-isothermal sheet flows has also been examined[21].

In this paper, we demonstrate that heating a Newtonian liquid sheet in the drawing process enhances its stability, and this increase can be dramatic. To this end, we impose a Gaussian heating profile followed by a region of cooling — to mimic a temperature profile that would be achieved in practice if a liquid sheet were only heated over part of its length. We demonstrate that a relatively narrow region of heating relative to the sheet length suppresses the classical draw resonance instability and increases the critical draw ratio by many orders of magnitude compared with that of an isothermal Newtonian flow. We demonstrate that the cooling profile that follows the Gaussian has a quantitative but relatively small effect on the magnitude of the critical draw ratio.

The organization of this paper is as follows. We first consider the limit of negligible heat transfer resistances in Sections II-III. In section II, the time dependent equations governing a viscous and thinning liquid sheet with variable viscosity are presented. The steady-state solution is provided as well as the linearized equations used to examine the stability of the steady flow. An eigenvalue problem is derived to determine the critical draw ratio, and its numerical solution is subsequently provided. Section III provides typical stability results

that demonstrate the key features of the temperature profile that lead to enhanced stability. In section IV, the effect of heat transfer resistances on stability results is examined, and concluding comments are provided in Section V.

II. FORMULATION: NEGLIGIBLE HEAT TRANSFER RESISTANCES

A. Sheet model and stability problem

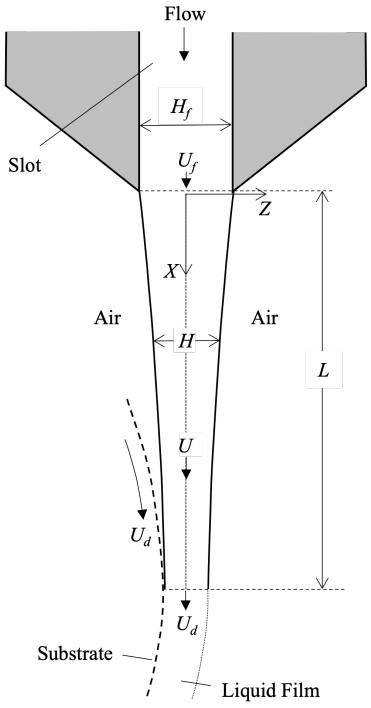

FIG. 1. Side view schematic of a liquid sheet of length L exiting a slot of height H_f and drawn onto a solid substrate (here shown as a portion of a curved roller) moving at speed U_d. The curtain is assumed to be infinite and invariant in the Y direction (oriented out of the figure) and is symmetrical about the line $Z = 0$. The local speed and thickness of the curtain are denoted as U and H, respectively.

Consider flow configuration shown in Figure 1 that depicts a planar liquid sheet of length, L, extruded from a slot of height, H_f, and drawn onto a substrate moving at speed, U_d. The sheet is invariant with the Y-direction (oriented out of Figure 1), with the X coordinate denoting distance down the sheet. The sheet itself has density, ρ, viscosity, η, and local thickness $H(X,t')$, where t' is time. We assume that the film is symmetrical about its centerline (i.e., the $Z = 0$ axis in Figure 1) and that the sheet thins gradually in the X-direction; this is afforded by the assumption that $H_f/L \ll 1$. As a result, the lack of viscous traction with the air enables an approximation that the fluid speed is locally plug (Z-independent in Figure 1) and can thus be expressed as $U(X,t')$. In making the plug flow assumption, end effects near the slot and substrate are neglected, where the loss/gain of traction creates local flow rearrangement not captured in a plug assumption. In what follows, we assume that the viscous forces dominate inertial, gravity, and surface tension forces; in this limit, end effects are expected to dissipate on the order of $5 - 10 \times H_f$ from the top and bottom of the curtain. In light of the $H_f \ll L$ assumption made, end effects are thus limited to small regions in the vicinity of $X = 0$ and $X = L$; any asymmetry in the curtain due to the substrate motion is embedded in the end effect near $x = L$. For this reason, the velocity of the planar sheet is taken to be equal to $U = U_f$ and $U = U_d$ at the top and bottom of the sheet, respectively. These constraints can be justified formally by an asymptotic match between the gradually thinning and rearrangement regions near the ends of the sheet.

We define dimensionless variables and parameters as:

$$\begin{aligned} h = H/H_f, \quad u = U/U_f, \quad t = t'U_f/L, \\ x = X/L, \quad D = U_d/U_f, \quad \mu = \eta/\eta_r. \end{aligned} \tag{1a}$$

In (1a), η_r is a reference viscosity that is related to the temperature field prescribed in section II B. Subject to the above-stated assumptions, the dimensionless boundary value problem governing the flow in the liquid sheet is:[27]

$$\frac{\partial h}{\partial t} + \frac{\partial (hu)}{\partial x} = 0, \qquad \frac{\partial}{\partial x}\left(\mu h \frac{\partial u}{\partial x}\right) = 0, \tag{1b}$$

$$h(0,t) = 1, \quad u(0,t) = 1, \quad u(1,t) = D = \exp(\beta). \tag{1c}$$

In (1), D is the draw ratio, and $\beta = \ln(D)$ is introduced in (1c) for convenience. Note that there is no initial condition specified as we intend to assess the stability of the flow with respect to arbitrary disturbances.

Under steady state conditions, which are denoted here with the subscript "0", the solution to (1) is given as:

$$u_0(x) = \exp(\beta f(x)), \qquad h_0 = \exp(-\beta f(x)), \tag{2a}$$

where

$$f(x) = \frac{\int_0^x 1/\mu(s)ds}{\int_0^1 1/\mu(s)ds}, \quad \beta = \ln(D). \tag{2b}$$

In (2b), the form of the dimensionless viscosity, μ is as of yet unspecified, but will be prescribed based on a location-dependent temperature profile in Section II B. We assess the system stability by linearizing equations (1) about the steady state solution (2) and examining the growth of arbitrary disturbances. The disturbances are assumed to have the form

$$h = h_0(1 + \alpha(x)e^{\lambda t}), \qquad u = u_0(1 + \phi(x)e^{\lambda t}), \tag{3}$$

where the perturbation functions satisfy $\alpha(x)$, $\phi(x) \ll 1$, and λ is, in general, a complex constant. At this stage, all of these perturbed quantities are unspecified. Substituting equation (3) into (1) and neglecting terms that are quadratic or higher in α and ϕ, a linear differential eigenvalue problem arises to solve for the perturbation functions and eigenvalue λ as follows:

$$\lambda\alpha + e^{\beta f(x)}(\alpha_x + \phi_x) = 0, \tag{4a}$$

$$(\mu\phi_x)_x + \mu\beta f'(x)(\alpha_x + \phi_x) = 0, \tag{4b}$$

$$\text{with constraints:} \quad \alpha(0) = 0, \quad \phi(0) = 0, \quad \phi(1) = 0. \tag{4c}$$

The system (4a-c) indicates that the eigenvalue λ depends on the draw ratio, D, through its relationship to β in (2b). Disturbances grow or decay depending on whether Real(λ) > 0 or Real(λ) < 0, respectively. Of critical importance is the critical draw ratio defined as:

$$D_c = \max\{D : \text{real part of all eigenvalues, } \lambda \leq 0\}. \tag{4d}$$

In particular, it is desirable for D_c to be as large as possible so the drawing process is stable over a wide range of drawing speeds with $D < D_c$. We will discuss the numerical solution of the system (4) in Section II C.

B. Dependence of Viscosity on Temperature

The viscosity, μ, in the eigenvalue system (4) depends on temperature. In the first portion of this study (Sections II-III), we consider the limit where the external temperature field is imposed directly on and inside of the liquid curtain[25]. This removes considerations of heat transfer from the problem so that the underlying effect of viscosity changes can be examined explicitly. Section IV considers the effect of heat transfer resistances on stability results, and the establishes the parameter range where negligible heat transfer results are valid.

Here, we impose a viscosity dependence that is typical for glass manufacture, a potential application domain for the results we present. Within the temperature range $1673 - 2273$K, the viscosity of glass may be expressed as[16]

$$\mu(T) = A \exp\left(\frac{B}{CT}\right), \tag{5}$$

with typical parameters given by

$$A = 5.8 \times 10^{-8}\text{poise}, \qquad B = 515400 \text{ J/mol}, \qquad C = 8.314 \text{ J/mol} \cdot \text{K}, \tag{6}$$

where T is the temperature in Kelvin. In our study, we impose a Gaussian heating profile as

$$T(x) = T_0 + (T_{\max} - T_0) \exp\left(-\frac{(x - x_0)^2}{2\sigma_0^2}\right), \qquad 0 \le x \le x_1 \tag{7a}$$

followed by a cooling profile

$$T(x) = T_2 + (T_1 - T_2) \exp\left(-\frac{(x - x_1)^2}{2\sigma_1^2}\right), \qquad x_1 \le x \le 1 \tag{7b}$$

where

$$T_1 = T_0 + (T_{\max} - T_0) \exp\left(-\frac{(x_1 - x_0)^2}{2\sigma_0^2}\right). \tag{7c}$$

Figure 2 provides a schematic of the temperature field expressed quantitively by (7). As indicated, the profile equation (7) mimics the configuration where molten glass at temperature T_0 enters a heating unit placed along the upper portion of the liquid sheet in a film drawing process, followed by a region of cooling once the fluid is exposed to air but before being drawn onto the substrate at $x = L$. There are four parameters for the heating profile (7a): the standard deviation σ_0, the heating floor temperature T_0, the maximum temperature $T_{\max}$ and its dimensionless location x_0. For the cooling profile in (7b), σ_1 controls

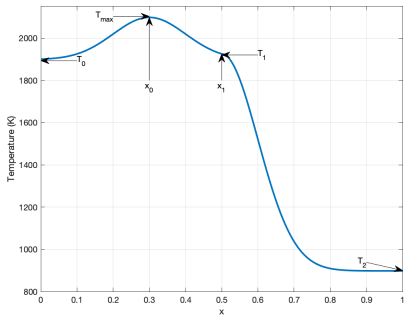

FIG. 2. Schematic of the temperature profile (7) with various parameters indicated. The the standard deviation in (7a), σ_0, affects the breadth of the indicated heating Gaussian, and σ_1, affects the slope of the cooling profile given by eq. (7b).

the cooling rate, T_2 is the cooling floor temperature, and x_1 is the dimensionless position at which the cooling begins.

We non-dimensionalize the temperature and viscosity profiles (eqs (5) and (7)) as follows. The heating floor temperature, T_0, is used as a scale for the temperature and the viscosity relation (5) is thus expressed in dimensionless form as

$$\mu(\theta) = \exp\left(\kappa\left(\frac{1}{\theta} - 1\right)\right), \tag{8a}$$

where the previously unspecified viscosity scale in (1a), η_r, is set as

$$\eta_r = A\exp(\kappa). \tag{8b}$$

The nondimensionalized form of the temperature field (7) is

$$\theta(x) = 1 + (\theta_{\max} - 1)\exp\left(-\frac{(x - x_0)^2}{2\sigma_0^2}\right), \qquad 0 \le x \le x_1 \tag{8c}$$

$$\theta(x) = \theta_2 + (\theta_1 - \theta_2)\exp\left(-\frac{(x - x_1)^2}{2\sigma_1^2}\right), \qquad x_1 \le x \le 1 \tag{8d}$$

where

$$\theta_1(x) = 1 + (\theta_{\max} - 1)\exp\left(-\frac{(x_1 - x_0)^2}{2\sigma_0^2}\right), \tag{8e}$$

and

$$\kappa = \frac{B}{CT_0}, \quad \theta_{\max} = \frac{T_{\max}}{T_0}, \quad \theta_2 = \frac{T_2}{T_0}. \tag{8f}$$

In (8a), μ depends on the function $\theta(x)$ which thus depends on 7 parameters: κ, $\theta_{\max}$, θ_2, x_0, x_1, σ_0 and σ_1. The critical draw ratio, D_c, extracted from the system (4), may be expressed functionally as

$$D_c = D_c(\kappa, \theta_{\max}, \theta_2, x_0, x_1, \sigma_0, \sigma_1). \tag{9}$$

Owing to the large number of parameters in (9), we have chosen to present the temperature field in dimensional form for ease of use and interpretation, and to demonstrate that the magnitude of the temperature profiles imposed are attainable in practice. All spatial quantities (i.e. $x, x_0,$ and x_1) are provided in dimensionless form. In what follows, we examine the dependence (9) to determine how the indicated parameters affect the system stability.

C. Solution for the critical draw ratio

The critical draw ratio, D_c, is determined by solving the eigenvalue system (4a-4c) with the viscosity dependence (8) and the criterion (4d). Here we will use the Chebyshev collocation method[14,29]. To begin, we discretize the differential eigenvalue system by representing the unknown continuous functions α and ϕ as column vectors,

$$\boldsymbol{\alpha} = \begin{bmatrix} \alpha_0 \\ \vdots \\ \alpha_n \end{bmatrix}, \qquad \boldsymbol{\phi} = \begin{bmatrix} \phi_0 \\ \vdots \\ \phi_n \end{bmatrix}. \tag{10}$$

where the as of yet undetermined vector components $(\alpha_i, \phi_i, i = 0, \ldots, n)$ are to be computed at the Chebyshev's points, $x_0, \ldots, x_n$,[29] of the domain, $x \in [0, 1]$. At the Chebyshev's points, eq. (4a-4b) can be approximated by the matrix equations

$$-\boldsymbol{S}\boldsymbol{D_x}\boldsymbol{\alpha} - \boldsymbol{S}\boldsymbol{D_x}\boldsymbol{\phi} = \lambda\boldsymbol{\alpha}, \tag{11a}$$

$$\boldsymbol{P}\boldsymbol{D_x}\boldsymbol{\alpha} + (\boldsymbol{D_{xx}} + (\boldsymbol{P} + \boldsymbol{M})\boldsymbol{D_x})\boldsymbol{\phi} = \boldsymbol{0}, \tag{11b}$$

where $\boldsymbol{S}$, $\boldsymbol{P}$ and $\boldsymbol{M}$ are diagonal matrices expressed as

$$\boldsymbol{S} = \mathrm{diag}(\exp(\beta(f(x_0)), \ldots, \exp(\beta f(x_n))), \tag{11c}$$

$$\boldsymbol{P} = \mathrm{diag}(\beta f'(x_0), \ldots, \beta f'(x_n)), \tag{11d}$$

$$\boldsymbol{M} = \mathrm{diag}(\mu'(x_0)/\mu(x_0), \ldots, \mu'(x_n)/\mu(x_n)). \tag{11e}$$

In (11), $\boldsymbol{D_x}$ is the Chebyshev differentiation matrix on the domain $[0,1]$, $\boldsymbol{D_{xx}} = \boldsymbol{(D_x)^2}$, and the prime denotes the x-derivative. In partitioned matrix notation, the system (11) can thus be written as

$$\left(\begin{array}{c|c} \boldsymbol{A_{11}} & \boldsymbol{A_{12}} \\ \hline \boldsymbol{A_{21}} & \boldsymbol{A_{22}} \end{array}\right)\left(\begin{array}{c} \boldsymbol{\alpha} \\ \hline \boldsymbol{\phi} \end{array}\right) = \lambda \left(\begin{array}{c|c} \boldsymbol{B_{11}} & \boldsymbol{B_{12}} \\ \hline \boldsymbol{B_{21}} & \boldsymbol{B_{22}} \end{array}\right)\left(\begin{array}{c} \boldsymbol{\alpha} \\ \hline \boldsymbol{\phi} \end{array}\right), \tag{12a}$$

where

$$\boldsymbol{A_{11}} = -\boldsymbol{S}\boldsymbol{D_x}, \qquad \boldsymbol{A_{12}} = -\boldsymbol{S}\boldsymbol{D_x}, \tag{12b}$$

$$\boldsymbol{A_{21}} = \boldsymbol{P}\boldsymbol{D_x}, \qquad \boldsymbol{A_{22}} = \boldsymbol{D_{xx}} + (\boldsymbol{P}+\boldsymbol{M})\boldsymbol{D_x}. \tag{12c}$$

In (12), $\boldsymbol{B_{11}}$ is an $(n+1)$ identity matrix, while $\boldsymbol{B_{12}}, \boldsymbol{B_{21}}$ and $\boldsymbol{B_{22}}$ are $(n+1)\times(n+1)$ zero matrices.

In discretized form, some slots of the column vectors $\boldsymbol{\alpha}$ and $\boldsymbol{\phi}$ have known quantities according from the boundary conditions (4c). In particular, we have $\alpha_n = \alpha(0) = 0, \phi_n = \phi(0) = 0$, and $\phi_0 = \phi(1) = 0$. As a result, the last rows of the matrix system in (11a-11b) and first row of (11b) are ignored. The reduced system can be placed in the form of Eq. (12) after modifying the matrices in MATLAB notation as:

$$\tilde{\boldsymbol{A}}_{\boldsymbol{11}} = \boldsymbol{A_{11}}(1:n, 1:n), \qquad \tilde{\boldsymbol{A}}_{\boldsymbol{12}} = \boldsymbol{A_{12}}(1:n, 2:n), \tag{13a}$$

$$\tilde{\boldsymbol{A}}_{\boldsymbol{21}} = \boldsymbol{A_{21}}(2:n, 1:n), \qquad \tilde{\boldsymbol{A}}_{\boldsymbol{22}} = \boldsymbol{A_{22}}(2:n, 2:n), \tag{13b}$$

$$\tilde{\boldsymbol{B}}_{\boldsymbol{11}} = \mathrm{eye}(n,n), \qquad \tilde{\boldsymbol{B}}_{\boldsymbol{12}} = \mathrm{zeros}(n, n-1), \tag{13c}$$

$$\tilde{\boldsymbol{B}}_{\boldsymbol{21}} = \mathrm{zeros}(n-1, n), \qquad \tilde{\boldsymbol{B}}_{\boldsymbol{22}} = \mathrm{zeros}(n-1, n-1), \tag{13d}$$

$$\tilde{\boldsymbol{\alpha}} = \boldsymbol{\alpha}(1:n), \qquad \tilde{\boldsymbol{\phi}} = \boldsymbol{\phi}(2:n). \tag{13e}$$

Note that eq. (12) is a generalized eigenvalue problem with a singular right hand side; it can be solved by the well-known QZ-algorithm[20]. We use $[U, E] = \mathrm{eig}(A, B, \text{'qz'})$ in MATLAB to solve the modified system to obtain the eigenvectors, U, and eigenvalues, E. A sequential refinement of the number of collocation points, n, was performed; an accuracy of $O(10^{-10})$ for all presented results was achieved for $n = 256$.

The stability of the viscous planar sheet depends on the real part λ in the perturbation form (3). According to (4d), we adjust the draw ratio until the real part of all eigenvalues are less than or equal to 0; the critical draw ratio arises when the maximum value of Real(λ) over all eigenvalues equals 0. As the original problem is real, all eigenvalues will arise as

complex conjugates. We use Brent's method,[4] a hybrid of the bisection and secant methods, to adjust the draw ratio to its critical value.

The Chebyshev collocation method computes the full spectrum of the eigenvalue problem for each choice of $\beta = \ln(D)$, and typical spectral results are shown in Figures 3a-c. These figures correspond to three different heating temperature profiles with different values of σ_0 in (8). In each figure, the critical eigenvalue is indicated with a star. When $\sigma_0 = 0.25$ (Figure 3a), the critical eigenvalue has its imaginary part closest to the real axis. As σ_0 is decreased to 0.125 (Figure 3b), the position of the critical eigenvalue moves away from the real axis and shifts position with one that was previously unstable at a lower value of σ_0. When $\sigma_0 = 0.075$ (Figure 3c), the relative location of the critical eigenvalue switches once again.

In previous work for isothermal[12] or cooled[21,23,25] planar liquid sheets, the eigenvalue spectrum that arises always has a qualitative form as in Figure 3a; prior work utilizes a shooting method, in which a previously determined critical eigenvalue is used as an initial guess as the draw ratio is changed. It is apparent from Figures 3b,c that the shooting approach could potentially lead to an invalid stability conclusion because the algorithm could converge to an incorrect eigenvalue attributed to criticality. For purposes of comparison, we did implement a shooting method (Appendix B) and indeed demonstrated that this behavior can happen. Note that from the shooting method did serve as a self-consistency check on our calculations, as it mapped out the eigenvalue predictions from the Chebyshev method as initial guesses for shooting were varied.

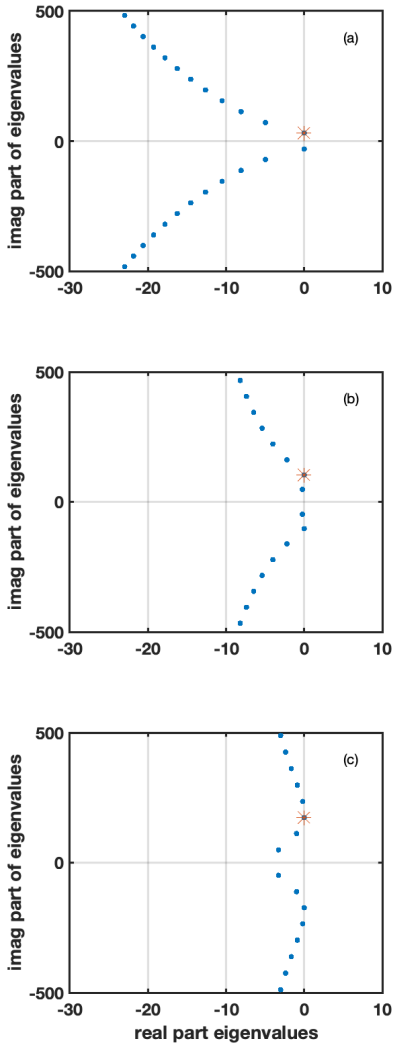

FIG. 3. Spectra correspond to three different temperature profiles for $T_0 = 1898$K, $T_{\max} - T_0 = 120$K, $\sigma_1 = 0.1$, $T_2 - T_0 = 1000$K, $x_0 = 0.2$, $x_1 = 0.6$. (a): $\sigma_0 = 0.25$, (b): $\sigma_0 = 0.125$, (c): $\sigma_0 = 0.075$. The $*$ plot symbol indicates the critical eigenvalue.

III. RESULTS: NEGLIGIBLE HEAT TRANSFER RESISTANCES

A. Effect of Temperature profiles on draw ratio

To begin, we examine the cooling portion of the temperature profiles in Figure 2 alone and examine the effect of heating subsequently. This serves two purposes. First, we demonstrate that our predictions are consistent with prior literature results that show the effect of cooling on the critical draw ratio[21,23,25]. Second we determine the order of magnitude of the effect of cooling, which provides a baseline for comparison when heating is added. To this end, we examine the stability of flows using the sequence temperature profiles shown in Figure 4; corresponding parameter values are provided in Table I. Additionally, Table I contains the critical draw ratios for all curves calculated following the numerical algorithm of section II C.

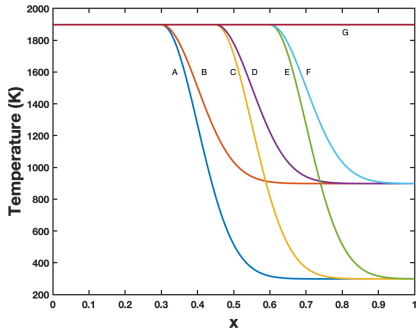

FIG. 4. Various cooling temperature profiles corresponding to parameters in Table I, which also contains the calculated critical draw ratios associated with each curve.

TABLE I. Data used in equation (7) to generate temperature profiles shown in Figure 4, with $T_0 = 1898$K and $T_{\max} - T_0 = 0$. Corresponding critical draw ratios, D_c, are indicated in the table.

Cooling Only				
Case	σ_1	x_1	$T_0 - T_2$	D_c
A	0.1	0.3	1600	20.98
B	0.1	0.3	1000	20.61
C	0.1	0.45	1600	20.87
D	0.1	0.45	1000	20.55
E	0.1	0.6	1600	20.61
F	0.1	0.6	1000	20.42
G	–	–	0	20.21

Consistent with previously cited literature,[25] the critical draw ratios shown in Table I are approximately 20 and insensitive of the cooling rate, σ_1, the cooling floor temperature, T_2 and the starting cooling location, x_1. If the viscosity is constant spatially (this corresponds to an isothermal flow as shown in curve G of Figure 4), $f(x) = x$ and $f'(x) = 1$ in eq. (2), and the velocity field is given analytically as $U = \exp(\beta x)$; as shown in Table I, we find $D_c = 20.21$, in agreement with previous literature[5,11,22,26].

With the effect of cooling examined and calibrated to prior literature, we now proceed to examine the effect of heating. As stated previously and shown in Figure 2, we utilize a Gaussian profile in the heating region according to Eq. (7a). Note that we did explore the effect of non-Gaussian profiles that had a flattened maximum temperature over a specific length; results are provided in Appendix A. While there is some quantitative benefit of such profiles to increase the critical draw ratio, the order of magnitude increase is similar to that of a Gaussian. Thus, a Gaussian was chosen for simplicity in the remainder of the paper.

Figure 5 provides some typical Gaussian heating profiles followed by isothermal or cooling conditions; these correspond to parameter values in Table II. Compared with typical isothermal or cooling profiles in Figure 4 — for which the critical draw ratio is ≈ 20 (see D_c values in Table I) — it is evident that heating the viscous sheet provides a significant increase in the critical draw ratio (see D_c values in Table II). This data clearly shows that as the height of the Gaussian increases (higher temperature), the critical draw ratio increases.

If the sheet is cooled following the heating region, the critical draw ratio is reduced, although it remains the same order of magnitude as for heating alone.

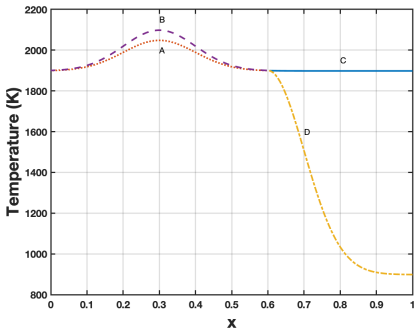

FIG. 5. Temperature profiles corresponding to data provided in Table II. Shown are Gaussian heating profiles (A or B) followed by either cooling (D) or isothermal (C). The aggregate heating/cooling/isothermal profiles are defined as AC, AD, BC, BD. Calculated critical draw ratios for all curves are provided in Table II.

TABLE II. Data used in equation (7) to generate temperature profiles shown in Figure 5, with $T_0 = 1898$K, $\sigma_0 = 0.1$, $\sigma_1 = 0.1$, $x_0 = 0.3$, $x_1 = 0.6$. Corresponding critical draw ratios, D_c, are indicated in the table.

Heating With and Without Cooling			
Case	$T_{\max} - T_0$	$T_0 - T_2$	D_c
AC	150	0	3.81×10^4
AD	150	1000	2.75×10^4
BC	200	0	8.37×10^6
BD	200	1000	4.75×10^6

We also find that or a given fixed heating profile, the magnitude of the critical draw ratio is relatively insensitive the cooling profile that follows (see Figure 6 and Table III).

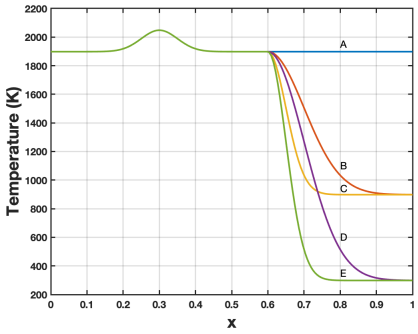

FIG. 6. Temperature profiles corresponding to data provided in Table III. Shown is a Gaussian heating profile followed by a sequence of cooling or isothermal profiles. Calculated critical draw ratios corresponding to each curve are provided in Table III.

TABLE III. Data used in equation (7) to generate temperature profiles shown in Figure 6, with $T_0 = 1898\text{K}$,$\sigma_0 = 0.1, T_{\max} - T_0 = 150, x_0 = 0.3, x_1 = 0.6$. Corresponding critical draw ratios, D_c, are indicated in the table.

Same Heating, Different Cooling Profiles			
Case	σ_1	$T_0 - T_2$	D_c
A	–	0	3.81×10^4
B	0.05	1000	2.65×10^4
C	0.10	1000	2.63×10^4
D	0.05	1600	2.75×10^4
E	0.10	1600	2.75×10^4

Figure 7 shows temperature profiles for different cooling zone lengths corresponding to parameters shown in Table IV. In accordance with Figure 2 and eq (7), x_1 is the heating zone length and $1 - x_1$ is the cooling zone length. Here we provide results for the same standard deviation and the location of the maximum temperature relative to the heating zone length. Inspection of Table IV shows that the order of magnitude of the D_c values is relatively insensitive to the cooling profile (compared the isothermal case of $D_c = 20.21$); that said, it is evident that a smaller heating zone length compared with that for cooling does quantitatively increase D_c. Note that in Figure 7, parameters for the Gaussian heating position, the standard deviation, and the length of the cooling zone are varied. Plots shown in the next section (Section III B) indicate that the increase in the standard deviation in the Gaussian heating profile, σ_0, is largely responsible for the trend in the critical draw ratios seen in Table IV.

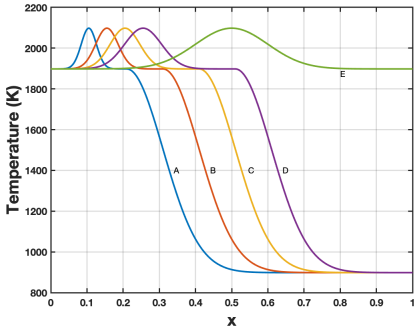

FIG. 7. Temperature profiles corresponding to data provided in Table IV. Shown are profiles having different cooling zone lengths and the same Gaussian heating profile scaled with heating zone length. Calculated critical draw ratios are provided in Table IV.

TABLE IV. Data used in equation (7) to generate temperature profiles shown in Figure 7, with $T_0 = 1898$K, $\sigma_0 = 0.1 \times x_1$, $x_0 = 0.5 \times x_1$, $\sigma_1 = 0.1$, $T_{\max} - T_0 = 200$, $T_2 - T_0 = 1000$.

Different Cooling Zone Lengths				
Case	σ_0	x_0	x_1	D_c
A	0.026	0.13	0.26	6.00×10^5
B	0.036	0.18	0.36	5.15×10^5
C	0.046	0.23	0.46	5.12×10^5
D	0.056	0.28	0.56	4.85×10^5
E	0.1	0.5	1.0	4.22×10^5

B. Survey of temperature profiles and stability enhancement

Section III A results show typical trends in the critical draw ratio as temperature profiles in the planar sheet are altered. These results indicate that the Gaussian heating profile is responsible for significant stability enhancement, and that cooling profiles alone do not lead to significant changes in the critical draw ratio compared with the classical isothermal case. In what follows, we provide a survey of parameters shown in Figure 2 that correspond to Gaussian heating — with and without subsequent cooling profiles — to more fully examine their effect on the critical draw ratio.

Figure 8a provides a contour plot of $\beta_c = \ln(D_c)$ as a function of the temperature increase in the Gaussian, $T_{\max} - T_0$ (see Figure 2), and its standard deviation, σ_0. Here the maximum temperature in the Gaussian, $T_{\max}$, is fixed as is the cooling profile. Temperature profiles corresponding to specific points A-E labeled in the contour plot (Figure 8a) are shown Figure 8b.

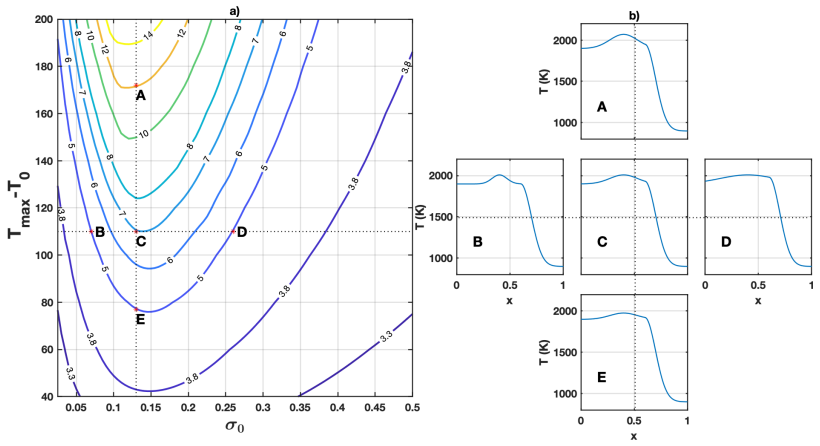

FIG. 8. a) Contour plot of the critical draw ratio, $\beta_c = \ln(D_c)$, as a function of the temperature rise in the Gaussian, $T_{\max} - T_0$, and its standard deviation, σ_0. Here, the Gaussian is fixed at $x_0 = 0.4$, and the cooling profile is fixed with $x_1 = 0.6$, $\sigma_1 = 0.1$, and $T_2 - T_0 = 1000K$. b) Temperature profiles corresponding to specific points A-E from Figure 8a are indicated.

Figure 8 shows that the largest critical draw ratios occur when σ_0 is about 0.15, and that increasing the height of the Gaussian (i.e., $T_{\max} - T_0$) increases the critical draw ratio dramatically (recall that $D_c = \exp(\beta_c)$).

Figure 9 provides data analogous to that of Figure 8 except the cooling profile has been eliminated; the Gaussian heating profiles, however, are identical (compare Figures 8b and 9b). We see that the structure of the parameter space is largely the same, with the maximum in the critical draw ratio arising for σ_0 in the range 0.1-0.15. As in Figure 8a, the critical draw ratio increases with increasing height of the Gaussian ($T_{\max} - T_0$).

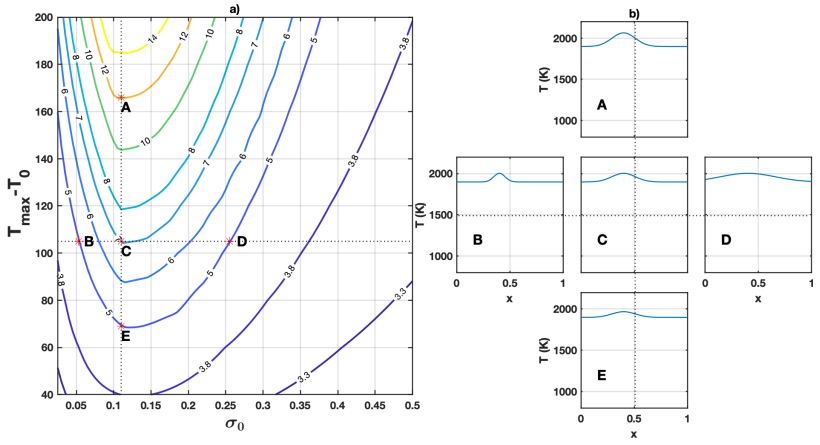

FIG. 9. a) Contour plot of the critical draw ratio, $\beta_c = \ln(D_c)$, as a function of the temperature rise in the Gaussian, $T_{\max} - T_0$, and its standard deviation, σ_0. Here, the Gaussian is fixed at $x_0 = 0.4$, and the cooling profile is fixed with $x_1 = 1$, $\sigma_1 = 0.1$, and $T_2 - T_0 = 1000K$. b) Temperature profiles corresponding to specific points A-E shown in the draw ratio contours are indicated.

As previously demonstrated in Section III, the Gaussian heating profile — not the cooling profile — is responsible for significant growth. This is reinforced by comparing the contours from Figures 8a (heating and cooling) and 9a (heating only), which have quantitative differences but are largely similar in structure. For this reason, we examine the effect of the location of the Gaussian temperature peak without cooling by comparing Figure 9 ($x_0 = 0.4$), Figure 10 ($x_0 = 0.5$), and Figure 11 ($x_0 = 0.6$). We see that for any height of the Gaussian ($T_{\max} - T_0$), moving the maximum peak to larger x value slightly increases the standard deviation for which the maximum benefit of heating is achieved. That said, the qualitative effect of the Gaussian heating is unchanged with location.

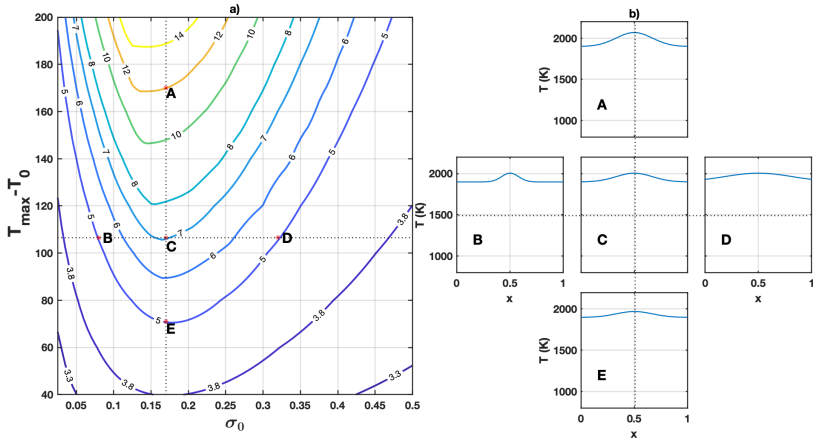

FIG. 10. a) Contour plot of the critical draw ratio, $\beta_c = \ln(D_c)$, as a function of the temperature rise in the Gaussian, $T_{\max} - T_0$, and its standard deviation, σ_0. Here, the Gaussian is fixed at $x_0 = 0.5$, and the cooling profile is fixed with $x_1 = 1$, $\sigma_1 = 0.1$, and $T_2 - T_0 = 1000K$. b) Temperature profiles corresponding to specific points A-E shown in the draw ratio contours are indicated.

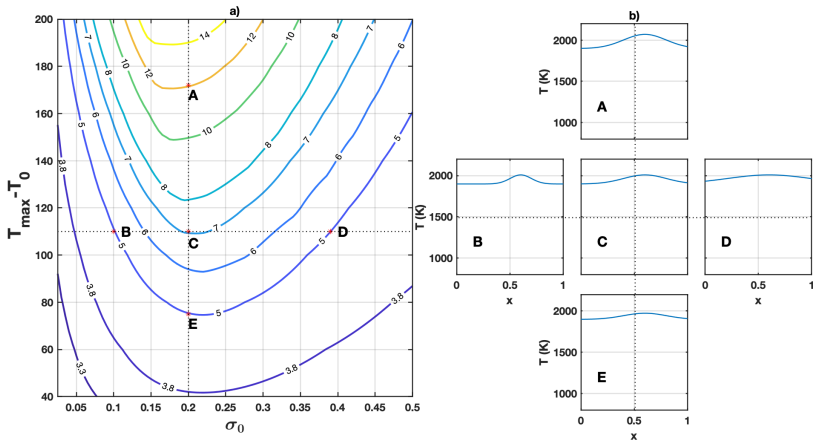

FIG. 11. a) Contour plot of the critical draw ratio, $\beta_c = \ln(D_c)$, as a function of the temperature rise in the Gaussian, $T_{\max} - T_0$, and its standard deviation, σ_0. Here, the Gaussian is fixed at $x_0 = 0.6$, and the cooling profile is fixed with $x_1 = 1$, $\sigma_1 = 0.1$, and $T_2 - T_0 = 1000K$. b) Temperature profiles corresponding to specific points A-E shown in the draw ratio contours are indicated.

Coupled with the survey of parameter values in Figure 8, the data of Section III demonstrates that heating before cooling increases the critical draw ratio and hence the stability of the liquid sheet. Figures 9-11 also show that the enhancement in stability originates from the heating profile, as cooling alone does not have a significant effect on the critical draw ratio compared with an isothermal configuration (see data in Figure 4 and Table I). The stability of the drawing process is relatively insensitive to the length of cooling zone when we choose the same standard deviation and the location of the maximum temperature relative the the length of the heating zone (see Figure 7). Our survey of parameter values indicates that the maximum stability of the liquid sheet occurs when the standard deviation of the Gaussian region of heating is relatively small compared with the length of the imposed heating zone.

IV. EFFECT OF HEAT TRANSFER RESISTANCES ON CRITICAL DRAW RATIO

In sections II and III, we examined the effect of heating a viscous liquid sheet in the limit of negligible heat transfer resistances. We now incorporate the effect of heat transfer to assess its impact on stability trends elucidated previously. Following the derivation by Scheid et. al.[25], the dimensionless thermal equation is given as

$$\frac{\partial \theta}{\partial t} + u\frac{\partial \theta}{\partial x} = -St\frac{\theta - T_a(x)}{h(1+(Bi/6)h)} \tag{14}$$

where θ is the dimensionless temperature, T_a is the dimensionless temperature of the ambient away from the curtain (scale used is T_0), $St = \frac{2L\alpha}{\rho c_p U_f H_f}$ is the Stanton number, $Bi = \frac{\alpha H_f}{k}$ is Biot number, and α is the heat transfer coefficient of the ambient. Additionally, k and c_p are the respective thermal conductivity and the heat capacity of the liquid. Equation (14) is coupled to the previously used equation set (1) to provide governing equations that incorporate heat transfer resistances in the sheet and externally. The functionality given by (9) is extended to add St and Bi as

$$D_c = D_c(St, Bi, \kappa, \theta_{\max}, \theta_2, x_0, x_1, \sigma_0, \sigma_1). \tag{15}$$

The solution of the heat transfer model to find the critical draw ratio closely follows the approach taken in Section II, and is provided in Appendix D.

In the limit of large St, equation (14) indicates that the dimensionless temperature, $\theta \sim T_a(x)$, and this indicates that the form of $T_a(x)$ should be chosen to be consistent with that given by equation (8) — this assures that our results for negligible heat transfer in section III are approached in the large St limit. To this end, we express a heating profile

$$T_a(x) = 1 + (\theta_{\max} - 1)\exp\left(-\frac{(x-x_0)^2}{2\sigma_0^2}\right), \qquad 0 \le x \le x_1 \tag{16a}$$

followed by a cooling profile

$$T_a(x) = \theta_2 + (\theta_1 - \theta_2)\exp\left(-\frac{(x-x_1)^2}{2\sigma_1^2}\right), \qquad x_1 \le x \le 1 \tag{16b}$$

where

$$\theta_1 = 1 + (\theta_{\max} - 1)\exp\left(-\frac{(x_1-x_0)^2}{2\sigma_0^2}\right). \tag{16c}$$

As in the negligible heat transfer resistance case, the viscosity dependence is given by (8a).

Figure 12 shows the effect of heat transfer resistances on the critical draw ratio as a function of Stanton and Biot numbers. We note that when St on the order of 10^4, heat transfer resistances are negligible, and the draw ratio is identical to that corresponding to curve BD in Figure 5 (as indicated in Table II). Note also that provided $St > 100$, the prediction without heat transfer resistances provides a lower bound on the critical draw ratio when heat transfer is included. The curve shapes in Figure 12 are relatively insensitive to the Biot number, and order of magnitude changes in Bi are required to significantly shift the curves. For this reason, the remaining data in this section is provided for $Bi = 0$.

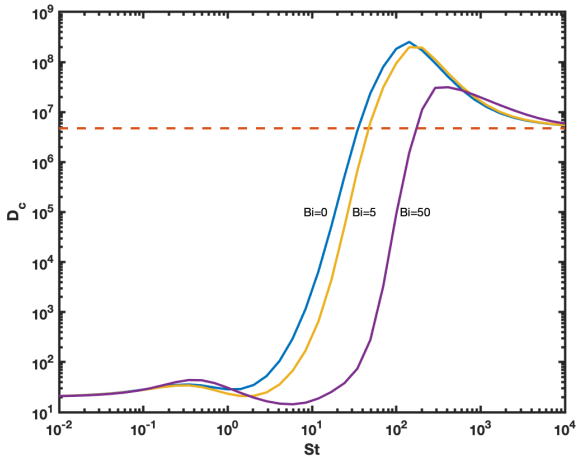

FIG. 12. Critical Draw Ratio, D_c, vs Stanton number, St, for various Biot numbers, Bi. The ambient temperature profile for all data in this figure corresponds to curve BD of Figure 5. The horizontal dashed line is the value of D_c corresponding to the case of negligible heat transfer. Parameters for the ambient temperature profile, given by (16), are: $x_0 = 0.3$, $x_1 = 0.6$, $\sigma_0 = 0.1$, $\sigma_1 = 0.1$, $T_0 = 1898$K, $T_{\max} = T_0 - 200$, $T_2 = T_0 - 1000$, and $\kappa = B/(CT_0) = 32.667$.

Figures 13-15 show the effect of heat transfer on the critical draw ratios obtained with no heat transfer resistances corresponding to curve BC in Figure 5 and curves D, E in Figure 7. Note that all critical draw ratios asymptote to the negligible heat transfer results for St on the order of 10^4. Additionally, for all cases, draw ratio results are comparable in magnitude to those without heat transfer at more moderate St values (approximately $St \approx 200$ and

larger).

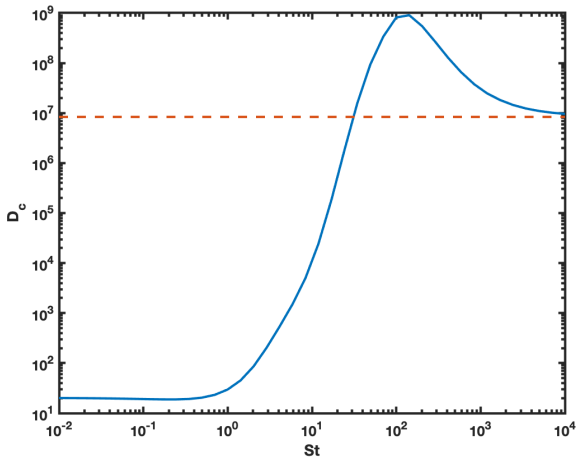

FIG. 13. Critical Draw Ratio, D_c, vs Stanton number, St, for the Biot number, $Bi = 0$. The ambient temperature profile for all data in this figure corresponds to curve BC of Figure 5. The horizontal dashed line is the value of D_c corresponding to the case of negligible heat transfer. Parameters for the ambient temperature profile, given by (16), are: $x_0 = 0.3$, $x_1 = 1$, $\sigma_0 = 0.1$, $\sigma_1 = 0.1$, $T_0 = 1898$K, $T_{\max} = T_0 - 200$, $T_2 = T_0 - 1000$, $\kappa = B/(CT_0) = 32.667$.

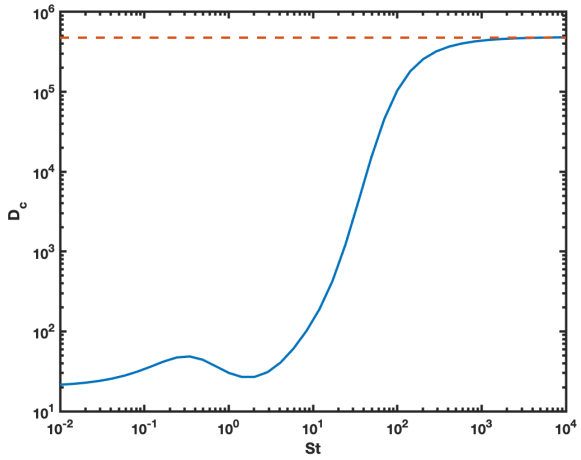

FIG. 14. Critical Draw Ratio, D_c, vs Stanton number, St, for the Biot number, $Bi = 0$. The ambient temperature profile for all data in this figure corresponds to curve D of Figure 7. The horizontal dashed line is the value of D_c corresponding to the case of negligible heat transfer. Parameters for the ambient temperature profile, given by (16), are: $x_0 = 0.28$, $x_1 = 0.56$, $\sigma_0 = 0.056$, $\sigma_1 = 0.1$, $T_0 = 1898$K, $T_{\max} = T_0 - 200$, $T_2 = T_0 - 1000$, $\kappa = B/(CT_0) = 32.667$.

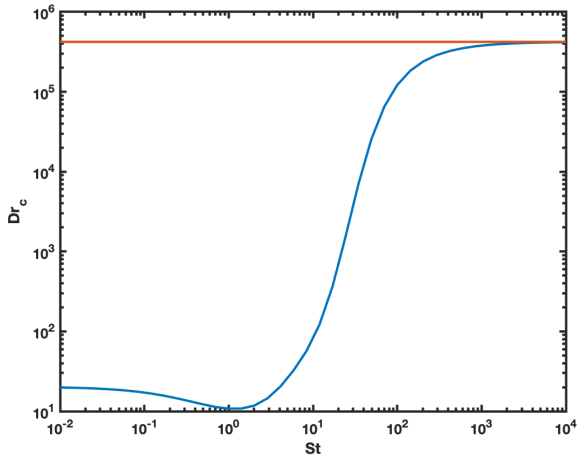

FIG. 15. Critical Draw Ratio, D_c, vs Stanton number, St, for the Biot number, $Bi = 0$. The ambient temperature profile for all data in this figure corresponds to curve E of Figure 7. The horizontal dashed line is the value of D_c corresponding to the case of negligible heat transfer. Parameters for the ambient temperature profile, given by (16), are: $x_0 = 0.5$, $x_1 = 1$, $\sigma_0 = 0.1$, $\sigma_1 = 0.1$, $T_0 = 1898$K, $T_{\max} = T_0 - 200$, $T_2 = T_0 - 1000$, $\kappa = B/(CT_0) = 32.667$.

V. CONCLUSION

In this paper, we have considered the effect of heating and cooling on the stability of a highly viscous and thin Newtonian sheet of liquid drawn onto a moving substrate under conditions of negligible inertial and gravity. Results of this paper have been presented predominantly in the limit of large Stanton number (internal and external heat transfer resistances are neglected), although the effect of heat transfer on presented results has been examined. Compared with an isothermal configuration, the critical draw ratio can be increased by many orders of magnitude depending on parameters of an imposed Gaussian heating profile. The observed stability enhancement is found to be less sensitive to the cooling profile after heating, although it does have a quantitative effect. We find that the maximum stability of the liquid sheet occurs when the standard deviation of the Gaussian region of heating is small compared with the length of the imposed heating zone. Our heat transfer analysis shows that the Stanton Number must be on the order of 10^4 for precise agreement with $St \to \infty$ numerics. As in the case of cooling,[25] there is a region of St over which significant enhancement on the critical draw ratio can be achieved. That said, our data shows that stability enhancements predicted without the heat transfer resistances are realizable at moderate Stanton numbers.

VI. DATA AVAILABILITY

The data that support the findings of this study are available within the article.

Appendix A: Additional Heating Profiles

In addition to the Gaussian heating profile used throughout this paper, we have examined other heating profiles. For all cases, we have found that a heating profile followed by cooling enhances stability compared with temperature profiles in which cooling alone is utilized. Figure A1a provides a plot of one such heating profile followed by the same cooling profile. Here, we provide data here corresponding to a temperature profile for a modified Gaussian with a flat top (a "Gaussian Hat" function). Figure A1b shows how the critical draw ratio is affected by the hat width, h_w. We see that the critical draw ratio of the Gaussian Hat function with small hat width is larger than that for a pure Gaussian heating profile,

although the benefit is ultimately lost for larger hat widths.

The Gaussian Hat function with hat width h_w is expressed quantitatively as:

$$T(x) = T_0 + (T_{\max} - T_0)\exp\left(-\frac{(x-x_0)^2}{2\sigma_0^2}\right), \qquad 0 \le x \le x_0 \tag{A.1a}$$

$$T(x) = T_{\max}, \qquad x_0 \le x \le x_0 + h_w \tag{A.1b}$$

$$T(x) = T_0 + (T_{\max} - T_0)\exp\left(-\frac{(x-x_0-h_w)^2}{2\sigma_0}\right), \qquad x_0 + h_w \le x \le x_1 \tag{A.1c}$$

$$T(x) = T_2 + (T_1 - T_2)\exp\left(-\frac{(x-x_1)^2}{2\sigma_1^2}\right), \qquad x_1 \le x \le 1 \tag{A.1d}$$

where

$$T_1 = T_0 + (T_{\max} - T_0)\exp\left(-\frac{(x_1-x_0-h_w)^2}{2\sigma_0^2}\right). \tag{A.1e}$$

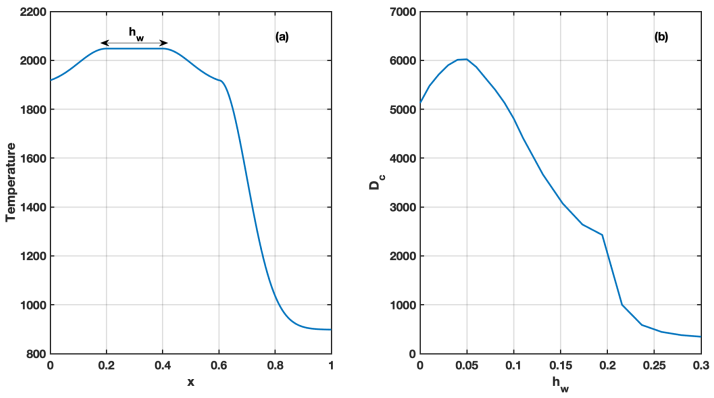

FIG. A-1. Gaussian hat heating profiles followed by cooling, and corresponding draw ratio results. A Gaussian heating profile is obtained when $h_w = 0$. (a) Temperature profile given by (A.1) with $x_0 = 0.2$, $x_1 = 0.6$, $h_w = 0.2$, $\sigma_0 = 0.1$, $\sigma_1 = 0.1$, $T_0 = 1898$, $T_{\max} = T_0 + 150$ and $T_2 = T_0 - 1000$. (b) Critical draw ratio, D_c, as a function of hat width, h_w.

Appendix B: Shooting Method to Solve the Eigenvalue Problem

Here, we provide a formulation of the shooting method approach to find eigenvalues. As stated in the main text, this is not a preferred method for finding eigenvalues when heating

profiles are imposed on the liquid sheet, as all eigenvalues are not predicted at one time as in the Chebyshev method — and errant conclusions about critical draw ratios may be drawn (see Section II.C). This statement is supported by a comparison between results of the two methods; additionally, we have established that the full Chebyshev spectrum can be obtained by altering the initial guesses in the shooting method, and this also serves as a self-consistency check on the Chebyshev numerics.

Let $P = \alpha, Q = \phi, R = \phi_x$ and $\bar{\mu} = 1/\int_0^1 \frac{ds}{\mu(s)}$ be the harmonic mean of the viscosity. We write the eigenvalue problem given by (4) as:

$$\frac{dP}{dx} = -\lambda P e^{-\beta f(x)} - R, \tag{B.1a}$$

$$\frac{dQ}{dx} = R, \tag{B.1b}$$

$$\frac{dR}{dx} = \frac{1}{\mu(x)}\left(-\mu_x R + \beta\bar{\mu}\lambda P e^{-\beta f(x)}\right), \tag{B.1c}$$

with initial conditions

$$P(0) = 0, \qquad Q(0) = 0. \tag{B.1d}$$

Since the system is linear, the eigenfunction is unique up to a scalar multiple. We set $R(0) = 1$ to fix the norm of the eigenfunction and make the system (B.1) well posed.

The algorithm proceeds as follows. For any value of λ, we numerically integrate the system to find $Q(1)$. The value of $Q(1)$ depends on λ so we define a function, $F(\lambda)$ as

$$F(\lambda) = Q(1). \tag{B.2}$$

The zeros of the equation $F(\lambda) = 0$ provide the eigenvalues, which are computed via the secant iteration method, expressed here as

$$\lambda_n = \lambda_{n-1} - F(\lambda_{n-1})\frac{\lambda_{n-1} - \lambda_{n-2}}{F(\lambda_{n-1}) - F(\lambda_{n-2})}. \tag{B.3}$$

We need two initial guesses, λ_0 and λ_1. As we see from typical spectra shown in Figure 3, the eigenvalues are complex, so at least one of the initial guesses must not be real. The iteration terminates when the norm of $F(\lambda)$ is less than a prescribed tolerance.

Appendix C: Heat Transfer Model

The model equations in dimensionless form are given by (1) and (14) with viscosity dependence (8a), rewritten here for ease of reference as a single system as:

$$h_t + (hu)_x = 0, \tag{C.1a}$$

$$(\mu h u_x)_x = 0, \tag{C.1b}$$

$$\theta_t + u\theta_x = -St\frac{\theta - T_a}{h(1 + (Bi/6)h)}, \tag{C.1c}$$

$$\mu(\theta) = \exp\left(\kappa\left(\frac{1}{\theta} - 1\right)\right). \tag{C.1d}$$

$$\text{B.C.} \qquad h(0,t) = 1 = u(0,t) = \theta(0,t), \quad u(1,t) = D. \tag{C.1e}$$

The parameters in (C.1) are the the Stanton number, St, the Biot number, Bi, the draw ratio, D, and the viscosity parameter, κ, defined in (8f). The ambient temperature away from the curtain, $T_a(x)$, is given by (16).

The steady state solutions, h_0, u_0 and θ_0 satisfy

$$(h_0 u_0)_x = 0 \tag{C.2a}$$

$$(\eta(\theta_0) h_0 u_{0x})_x = 0 \tag{C.2b}$$

$$u_0\theta_{0x} = -St\frac{\theta_0 - T_a}{h_0(1 + (Bi/6)h_0)}, \tag{C.2c}$$

with boundary conditions

$$h_0(0) = u_0(0) = \theta_0(0) = 1 \qquad \text{and} \qquad u_0(1) = D. \tag{C.2d}$$

The solution of the system (C.2) is given by

$$h_0 = \frac{1}{u_0} \tag{C.3a}$$

$$u_0' = \frac{u_0 f_0}{\eta(\theta_0)} \tag{C.3b}$$

$$\theta_0' = -\mathrm{St}\frac{\theta_0 - T_a}{(1 + (Bi/6)h_0)}, \tag{C.3c}$$

with $u_0(0) = 1$ and $\theta_0(0) = 1$. In (C.3b), f_0 is constant of integration that is determined by applying the boundary condition, $u_0(1) = D$ from (C.2d).

Next, we perturb about the base state (C.3) as

$$h(x,t) = h_0(1 + H(x)e^{\lambda t}), \tag{C.4a}$$

$$u(x,t) = u_0(1 + U(x)e^{\lambda t}), \tag{C.4b}$$

$$\theta(x,t) = \theta_0(1 + \Theta(x)e^{\lambda t}). \tag{C.4c}$$

where $H(x)$, $U(x)$ and $\Theta(x)$ are as of yet unknown functions and λ is the eigenvalue. Linearized equations are obtained by substituting (C.4) into (C.1) and neglecting terms quadratic or higher in the perturbed quantities to obtain

$$\lambda H + u_0(H_x + U_x) = 0, \tag{C.5a}$$

$$(\eta(\theta_0)U_x)_x + f_0\left(H_x + U_x - \kappa\left(\frac{\Theta}{\theta_0}\right)_x\right) = 0, \tag{C.5b}$$

$$\begin{aligned} \lambda\Theta + u_0\Theta_x + \frac{St}{\theta_0 h_0(1 + (Bi/6)h_0)} \\ \left[T_a\Theta - (\theta_0 - T_a)\left(U + \frac{1 + (Bi/3)h_0}{1 + (Bi/6)h_0}H\right)\right] = 0. \end{aligned} \tag{C.5c}$$

The boundary conditions for the perturbation functions are:

$$H(0) = U(0) = \Theta(0) = 0, \quad \text{and} \quad U(1) = 0. \tag{C.5d}$$

Note that steady solutions depends on the draw ratio D. The critical draw ratio is obtained numerically as described in the next section.

Appendix D: Chebyshev collocation method for heat transfer model

The critical draw ratio, D_c, is determined by solving the eigenvalue system (C.5) and the criterion (4d). The eigenvalue problem (C.5) is written in the following form:

$$\begin{bmatrix} \mathcal{A}_{11} & \mathcal{A}_{12} & \mathcal{A}_{13} \\ \mathcal{A}_{21} & \mathcal{A}_{22} & \mathcal{A}_{23} \\ \mathcal{A}_{31} & \mathcal{A}_{32} & \mathcal{A}_{33} \end{bmatrix} \begin{bmatrix} H \\ U \\ \Theta \end{bmatrix} = \lambda \begin{bmatrix} 1 & 0 & 0 \\ 0 & 0 & 0 \\ 0 & 0 & 1 \end{bmatrix} \begin{bmatrix} H \\ U \\ \Theta \end{bmatrix} \tag{D.1a}$$

where

$$\mathcal{A}_{11} = -u_0\frac{d}{dx}, \quad \mathcal{A}_{12} = -u_0\frac{d}{dx}, \quad \mathcal{A}_{13} = 0,$$

$$\mathcal{A}_{21} = \frac{f_0}{\eta}\frac{d}{dx}, \quad \mathcal{A}_{22} = \frac{d^2}{dx^2} + \left(\frac{f_0}{\eta} + \frac{\eta'}{\eta}\right)\frac{d}{dx},$$
$$\mathcal{A}_{23} = -\frac{f_0\kappa}{\eta}\frac{d}{dx}\frac{1}{\theta_0},$$
$$\mathcal{A}_{31} = \frac{St(\theta_0 - T_a)u_0}{\theta_0(1+(Bi/6)h_0)}\left(\frac{1+(Bi/3)h_0}{1+(Bi/6)h_0}\right),$$
$$\mathcal{A}_{32} = \frac{St(\theta_0 - T_a)u_0}{\theta_0(1+(Bi/6)h_0)},$$
$$\mathcal{A}_{33} = -\frac{StT_a u_0}{\theta_0(1+(Bi/6)h_0)} - u_0\frac{d}{dx}$$

with

$$B.C. \quad H(0) = 0, \quad U(0) = 0, \quad U(1) = 0, \quad \Theta(0) = 0. \tag{D.1b}$$

As in the case of negligible heat transfer resistances implemented in section II C, we utilize the Chebyshev collocation method[14,29]. To begin, we discretize the differential eigenvalue system by representing the unknown continuous functions H, U and Θ as column vectors,

$$\boldsymbol{H} = \begin{bmatrix} H_0 \\ \vdots \\ H_n \end{bmatrix}, \qquad \boldsymbol{U} = \begin{bmatrix} U_0 \\ \vdots \\ U_n \end{bmatrix}, \qquad \boldsymbol{\Theta} = \begin{bmatrix} \Theta_0 \\ \vdots \\ \Theta_n \end{bmatrix} \tag{D.2}$$

where the as of yet undetermined vector components $(H_i, U_i, \Theta_i, i = 0, \ldots, n)$ are to be computed at the Chebyshev's points, $x_0, \ldots, x_n$,[29] of the domain, $x \in [0, 1]$. The operators in (D.1a) are turned into matrices of order $(n+1) \times (n+1)$. The operators are either a function or a function multiplying an operator. We turn the function into a diagonal matrix of order $(n+1)$ whose diagonal elements are the function values at the Chebyshev points of the domain. For example, the operator $\mathcal{A}_{11}$ will become $-\text{diag}(u_0)\boldsymbol{D_x}$ and $\mathcal{A}_{23}$ will become $-\text{diag}\left(\frac{f_0\kappa}{\eta}\right)\boldsymbol{D_x}\text{diag}\left(\frac{1}{\theta_0}\right)$. The second derivative operator d/dx^2 becomes $\boldsymbol{(D_x)^2}$. At the Chebyshev's points, equations (C.5a)-(C.5c) can be approximated by the matrix equations

$$\begin{bmatrix} \boldsymbol{A}_{11} & \boldsymbol{A}_{12} & \boldsymbol{A}_{13} \\ \boldsymbol{A}_{21} & \boldsymbol{A}_{22} & \boldsymbol{A}_{23} \\ \boldsymbol{A}_{31} & \boldsymbol{A}_{32} & \boldsymbol{A}_{33} \end{bmatrix} \begin{bmatrix} \boldsymbol{H} \\ \boldsymbol{U} \\ \boldsymbol{\Theta} \end{bmatrix} = \lambda \begin{bmatrix} \boldsymbol{I} & \boldsymbol{0} & \boldsymbol{0} \\ \boldsymbol{0} & \boldsymbol{0} & \boldsymbol{0} \\ \boldsymbol{0} & \boldsymbol{0} & \boldsymbol{I} \end{bmatrix} \begin{bmatrix} \boldsymbol{H} \\ \boldsymbol{U} \\ \boldsymbol{\Theta} \end{bmatrix} \tag{D.3}$$

In discretized form, some slots of the column vectors $\boldsymbol{H}$, $\boldsymbol{U}$ and $\boldsymbol{\Theta}$ have known quantities according from the boundary conditions (C.5d). In particular, we have $H_n = H(0) = 0, U_n = U(0) = 0$, $U_0 = U(1) = 0$ and $\Theta_n = \Theta(0) = 0$. As a result, the $(n+1)$th and $(n+2)$th,

$(2n+2)$th and $(3n+3)$th rows of the matrix equation (D.3) are ignored. The reduced system can be placed in the form of Eq. (D.3) after modifying the matrices in MATLAB notation as:

$$\tilde{\boldsymbol{A}}_{\boldsymbol{11}} = \boldsymbol{A}_{\boldsymbol{11}}(1:n,1:n), \quad \tilde{\boldsymbol{A}}_{\boldsymbol{12}} = \boldsymbol{A}_{\boldsymbol{12}}(1:n,2:n), \quad \tilde{\boldsymbol{A}}_{\boldsymbol{13}} = \boldsymbol{A}_{\boldsymbol{13}}(1:n,1:n), \tag{D.4a}$$

$$\tilde{\boldsymbol{A}}_{\boldsymbol{21}} = \boldsymbol{A}_{\boldsymbol{21}}(2:n,1:n), \quad \tilde{\boldsymbol{A}}_{\boldsymbol{22}} = \boldsymbol{A}_{\boldsymbol{22}}(2:n,2:n), \quad \tilde{\boldsymbol{A}}_{\boldsymbol{23}} = \boldsymbol{A}_{\boldsymbol{23}}(2:n,1:n), \tag{D.4b}$$

$$\tilde{\boldsymbol{A}}_{\boldsymbol{31}} = \boldsymbol{A}_{\boldsymbol{31}}(1:n,1:n), \quad \tilde{\boldsymbol{A}}_{\boldsymbol{32}} = \boldsymbol{A}_{\boldsymbol{22}}(1:n,2:n), \quad \tilde{\boldsymbol{A}}_{\boldsymbol{33}} = \boldsymbol{A}_{\boldsymbol{33}}(1:n,1:n), \tag{D.4c}$$

$$\tilde{\boldsymbol{B}}_{\boldsymbol{11}} = \mathrm{eye}(n,n), \quad \tilde{\boldsymbol{B}}_{\boldsymbol{12}} = \mathrm{zeros}(n,n-1), \quad \tilde{\boldsymbol{B}}_{\boldsymbol{13}} = \mathrm{zeros}(n,n), \tag{D.4d}$$

$$\tilde{\boldsymbol{B}}_{\boldsymbol{21}} = \mathrm{zeros}(n-1,n), \quad \tilde{\boldsymbol{B}}_{\boldsymbol{22}} = \mathrm{zeros}(n-1,n-1), \quad \tilde{\boldsymbol{B}}_{\boldsymbol{23}} = \mathrm{zeros}(n-1,n), \tag{D.4e}$$

$$\tilde{\boldsymbol{B}}_{\boldsymbol{31}} = \mathrm{zeros}(n,n), \quad \tilde{\boldsymbol{B}}_{\boldsymbol{32}} = \mathrm{zeros}(n,n-1), \quad \tilde{\boldsymbol{B}}_{\boldsymbol{33}} = \mathrm{eye}(n,n), \tag{D.4f}$$

$$\tilde{\boldsymbol{H}} = \boldsymbol{H}(1:n), \quad \tilde{\boldsymbol{U}} = \boldsymbol{U}(2:n) \quad \tilde{\boldsymbol{\Theta}} = \boldsymbol{\Theta}(1:n). \tag{D.4g}$$

Note that eq. (D.3) is a generalized eigenvalue problem with a singular right hand side; it can be solved by the well-known QZ-algorithm[20]. We use $[U, E] = \mathrm{eig}(A, B, \text{'qz'})$ in MATLAB to solve the modified system to obtain the eigenvectors, U, and eigenvalues, E.

REFERENCES

[1]Acquaviva, M. R., Della Pia, A., Chiatto, M., and Luca, L.,'*Hole-driven dynamics of a three-dimensional gravitational liquid curtain*, J. Fluid Mech., vol. 968, A20, (2023),

[2]Andrews, J. H., *Cooling of a spinning thread-line*, Brit. J. Appl. Phys. 10, 39 (1959).

[3]Blake, T. D., Clarke, A., and Ruschak, K. J., *Hydrodynamic assist of dynamic wetting*, AIChE J. 40, 229, (1994).

[4]Brent, R. P., *Algorithms for Minimization without Derivatives*, Prentice-Hall, Englewood Cliffs, New Jersey, (1973).

[5]Chang, J. C and Denn, M. M., *An Experimental Study of Isothermal Spinning of a Newtonian and a Viscoelastic Liquid*, J. Non-Newtonian Fluid Mech., Vol. 5, 369-385, (1979).

[6]Chiatto, M. and Della Pia, A., *Natural frequency discontinuity of vertical liquid sheet flows at transcritical threshold*, J. Fluid Mech., vol. 945, A32, (2022).

[7]Della Pia, A., Colanera, A. and Chiatto, M., Surface tension-induced instability in spatially developing subcritical liquid curtains, Phys. Fluids 34, 042122 (2022).

[8]Della Pia, A., Chiatto, M. and L. Luca, *Varicose dynamics of liquid curtain: Linear analysis and volume-of-fluid simulations*, Phys. Rev. Fluids 9, 084003 (2024).

[9]Doremus, R. H., *Viscosity of silica*, Journal of Applied Physics 92, 7619, (2002).

[10]Fitt, A. D., Furusawa, K., Monro, T. M., Please, C. P., and Richardson, D. J., *The mathematical modelling of capillary drawing for holey fibre manufacture*, J. Eng. Math. 43(2/3), 201-227, (2002).

[11]Gelder, D., *The Stability of Fiber Drawing Processes*, Ind. Eng. Chem. Fund. Vol. 10, 534-535, (1971).

[12]Hagen, T., *Eigenvalue Asymptotics in Isothermal Forced Elongation* J. of Mathematical Analysis and Application, 244, 393-407 (2000)

[13]Hagen, T., *On the Effects of Spinline Cooling and Surface Tension in Fiber spinning* Z. Angew. Math. Mech. 82 vol. 8, 545-558, (2002).

[14]Hagen, T. and Langwallner, B., *A numerical study on the suppression of draw resonance by inertia* Z. Angew. Math. Mech. 86, No. 1, 63-70, (2006).

[15]Huber, C. M., Barlow, N. S. and Weinstein, S. J., *On the response of neutrally stable flows to oscillatory forcing with application to liquid sheets*, Phys. Fluids 34, 104106 (2022).

[16]Jasion, G. T., Hayes, J. R., Wheeler, N. V., Chen, Y., Bradley, T. D. , Richardson, D.

J. and Poletti, F., *Fabrication of tubular anti-resonant hollow core fibers: Modelling, draw dynamics and process optimization* Optical Express, Vol. 27, No. 15 (2019).

[17]Kase, S., Matsuo, T., *Studies on Melt Spinning. I. Fundamental Equations on the Dynamics of Melt Spinning*, J. Polym. Sci. A3, 2541 (1965).

[18]Kase, S., and Matsuo, T, *Studies on Melt Spinning: II Steady State and Transient Solution of Fundamental Equations Compared With Experiment Results*, J. Appl. Polymer Sci., Vol. 11, pp. 251-287, (1967).

[19]Matovich, M., and Pearson, J., *Spinning A Molten Threadline: Steady-State Isothermal Viscous Flows*, Ind. Eng. Chem., Fundam. 8, 512, (1969).

[20]Moler, C .B., and Stewart, G. W., *An algorithm for generalized matrix eigenvalue problems*, SIAM J. Numer. Anal. 10, 241-256, (1973).

[21]Philippi, J., Bechert, M., Chouffart, Q., Waucquez, C. and Scheid, B., *Linear stability analysis of nonisothermal glass fiber drawing*, Phys. Rev. Fluids 7, 043901, (2022).

[22]Pearson, J. and Matovich, M., *Spinning a Molten Threadline: Stability*, Ind. Eng. Chem., Fundam. 8, 605, (1969).

[23]Shan, Y. and Pearson, J., *On the stability of nonisothermal fiber spinning.* Ind. Eng, Chem. Fundam. 11, 145-149, (1972).

[24]Shan, Y. and Pearson, J., *On the stability of nonisothermal fiber spinning - general case.* Ind. Eng, Chem. Fundam. 11, 145-149, (1972).

[25]Scheid, B., Quiligotti, S., Tran, B., Gy, R. and Stone, H. A. *On the (de)stabilization of draw resonance due to cooling* J. Fluid Mech., vol. 636, pp. 155-176, (2009).

[26]Schultz, W. W. and Davis, S. H., *One Dimensional Liquid Fibers*, J. Rheol., Vol. 26, pp. 331-345, (1982).

[27]Schultz, W. W. and Davis, S. H., *Effects of Boundary Conditions on the Stability of Slender Viscous Fibers* Journal of Applied Mechanics, Vol. 51, 1-5, (1984).

[28]Torsey, B. M., Weinstein, S. J., Ross, D. S. and Barlow, N. S., *The effect of pressure fluctuations on the shapes of thinning liquid curtains*, J. Fluid Mech., vol. 910, A38, (2021).

[29]Trefethen, L. N., Spectral Methods in MATLAB, SIAM (2000).

[30]Weinstein, S. J. and Ruschak, K. J., *Coating Flows*, Annu. Rev. Fluid Mech., 36:29–53, (2004).

[31]Weinstein., S. J. and Gros, A., *Viscous liquid sheets and operability bounds in extrusion coating* Chemical Engineering Science 60, 5499 – 5512, (2005).

[32]Wylie, J., Huang, H. and Miura, R., *Thermal instability in drawing viscous threads* J. Fluid Mech., vol. 470, pp. 1-16, (2007).

[33]Yeow, Y. L.,, *On the stability of extending films: a model for the film casting process*, J. Fluid Mech., vol. 66, part 3, pp. 613-622, (1974).